# LPO predicted seismic anisotropy beneath a simple model of a mid-ocean ridge

S. E. J. Nippress,[1] N. J. Kusznir,[1] and J.-M. Kendall[2]

Received 6 March 2007; revised 19 May 2007; accepted 30 May 2007; published 21 July 2007.

[1] Modelling of seismic anisotropy in complex geodynamic environments is common. However the sensitivity of predicted seismic anisotropy and shear-wave splitting to mineral parameters is sometimes overlooked. We use a simple ocean ridge corner flow solution to investigate the effect of varying mineral parameters on the generation of seismic anisotropy and whether these differences can be detected by the predicted shear-wave splitting. We find that seismic anisotropy and shear wave splitting predicted using LPO theory is sensitive to mineral input parameters, such as grain boundary mobility, grain boundary sliding and mineral composition, however experimental constraints greatly reduce the range of predicted values. Predicted shear-wave splitting for a range of mineral parameters are consistent with observations at mid-ocean ridges. Although differences are seen in the predicted shear-splitting for different mineral parameters they are probably too small to detect in observations and hence will not give us new insights in to variation in mantle mineral properties. **Citation:** Nippress, S. E. J., N. J. Kusznir, and J.-M. Kendall (2007), LPO predicted seismic anisotropy beneath a simple model of a mid-ocean ridge, *Geophys. Res. Lett.*, *34*, L14309, doi:10.1029/2006GL029040.

## 1. Introduction

[2] Seismic anisotropy is now commonly modelled using a variety of different methods [e.g., *Blackman et al.*, 1996]. These methods generally require input information concerning the mineral or rock deformation properties of the anisotropic region and these can generate differences in the predicted seismic anisotropy models. However, most anisotropic modelling is conducted in complex geodynamic regions and so it is unclear whether differences due to different mineral/rock properties can be detected by the predicted shear-wave splitting. In this study we examine the sensitivity of predicted seismic anisotropy models and shear-wave splitting to changes in mineral parameters using a simple model of a mid-ocean ridge.

[3] Seismic anisotropy has been linked to mineral preferred orientation (also known as lattice preferred orientation (LPO) or texture) of anisotropic olivine crystals [*Nicolas and Christensen*, 1987]. *Chastel et al.* [1993] developed a finite element method that incorporates as a constitutive equation polycrystal plasticity, to investigate the development of LPO and hence seismic anisotropy in a convecting cell. *Blackman et al.* [1996] use the same method to investigate the nature of deformation associated with mantle upwelling in the upper 110km of the mantle at a mid-ocean ridge. Two methods of polycrystal plasticity (the lower bound deformation and the self consistent deformation) are used by *Blackman et al.* [2002] to calculate and then compare texture development beneath a mid-ocean ridge.

[4] Although dynamic recrystallization is important in the prediction of LPO in the mantle, only a small number of studies have incorporated this effect into their models. The first generation of methods for modelling LPO [e.g., *Jessell*, 1988] were based on the assumption that certain orientations were favoured during dynamic recrystallization. *Wenk and Tomé* [1999] and *Kaminski and Ribe* [2001] (hereinafter referred to as KR01) developed methods where the evolution of olivine LPO is generated by simultaneous plastic flow and dynamic recrystallization. *Blackman et al.* [2002] use a method that balances grain nucleation and grain growth, depending on deformation characteristics [*Wenk et al.*, 1997] to explore how grain growth and/or nucleation may affect the textures that develop along a streamline beneath a mid-ocean ridge.

[5] In this study, the theory of *Ribe and Yu* [1991] and KR01 for plastic deformation and dynamic recrystallization of polycrystalline aggregates is used to calculate lattice-preferred orientation models of seismic anisotropy within a simple mid-ocean ridge setting. Seismic rays are passed through these models to predict shear-wave splitting at the Earth's surface. We use a very simple geodynamic model so that we can investigate whether small changes in mineral input properties, such as grain boundary mobility, grain boundary sliding and mineral composition can be observed in predicted seismic anisotropy models, and perhaps more importantly in the predicted shear-wave splitting.

## 2. Modelling Mantle Flow Beneath a Mid-Ocean Ridge

[6] Temperature and stress dependant viscosity, buoyancy and melt significantly alter the pattern and amplitude of mantle flow and strain beneath a mid-ocean ridge [e.g., *Braun et al.*, 2000, *Blackman et al.*, 2002]. We use a simplified mantle flow field beneath a mid-ocean ridge derived from an iso-viscous corner flow model [e.g., *Phipps Morgan*, 1987] to allow the control of predicted seismic anisotropy by mineral deformation and composition to be isolated from the effects of temperature and stress dependant viscosity, buoyancy and melt included in more complex flow modelling.

[1]Department of Earth and Ocean Sciences, University of Liverpool, Liverpool, UK.
[2]Earth Sciences, University of Bristol, Bristol, UK.


0094-8276/07/2006GL029040$05.00

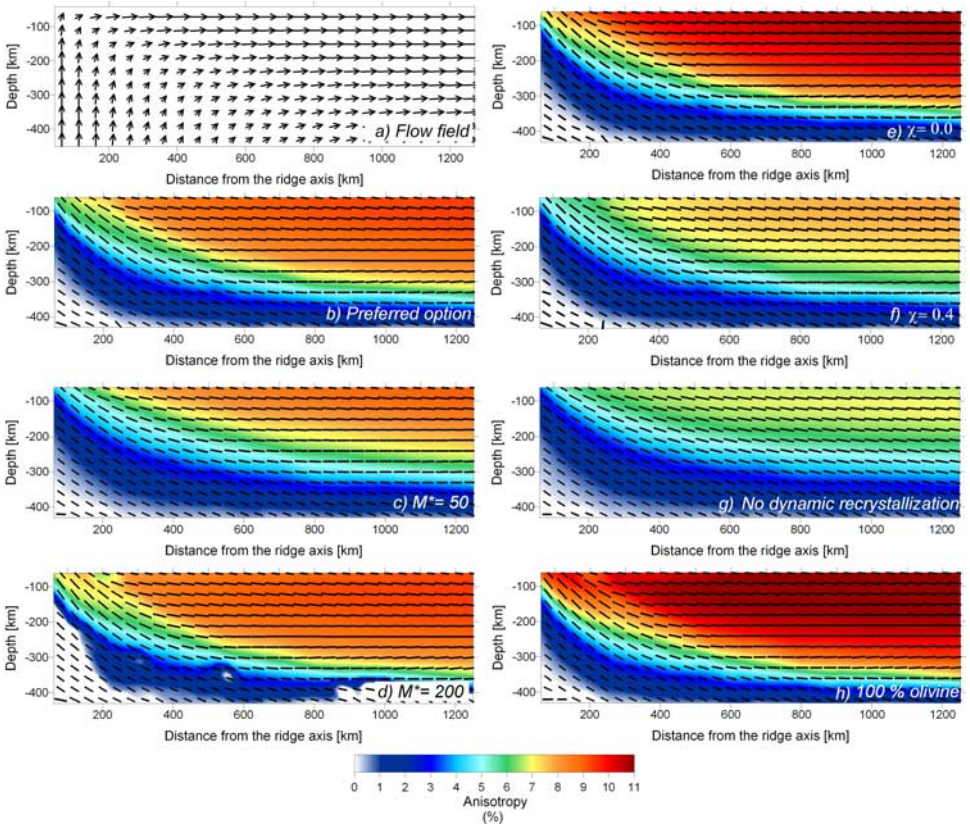


**Figure 1.** Predicted seismic anisotropy for a simple mid-ocean ridge model. (a) Simple corner flow model. (b–h) Sensitivity of seismic anisotropy to LPO input parameters at a mid-ocean ridge. Orientation of the hexagonal symmetry axis (black bars) and percentage of S-wave anisotropy (colour scale). Parameters are M* = 125, $\chi$ = 0.2, using dynamic recrystallization, and an aggregate composite comprising 70% olivine and 30% enstatite unless otherwise stated. Preferred parameters (Figure 1a), M* = 50 (Figure 1b), M* = 200 (Figure 1c), $\chi$ = 0.0 (Figure 1d), $\chi$ = 0.4 (Figure 1e), no dynamic recrystallization (Figure 1f) and 100% olivine aggregate (Figure g).

[7] The stream function, $\varphi$, for iso-viscous corner flow is defined as [*Batchelor*, 1967]:

$$\varphi = (\mathrm{A}x + \mathrm{B}z) + (\mathrm{C}x + \mathrm{D}z)\arctan(z/x) \quad (1)$$

where A, B, C, D are constants whose values are determined by the boundary conditions Vx the half spreading rate and Vz the axial upwelling velocity.

[8] The resulting flow field using Vx = 1 and Vz = $2/\pi$, corresponding to passive upwelling [*Phipps Morgan*, 1987] is shown in Figure 1a. Temperature and stress dependant viscosity, and buoyancy focus upwelling under the ocean ridge axis leading to higher Vz/Vx ratios. We have tested model predictions for $V_Z/V_X$ up to 5 and find that the pattern of predicted seismic anisotropy is similar to that for Vz/Vx = $2/\pi$, however the magnitude of the anisotropy decreases with increasing Vz/Vx.

## 3. Predicting Seismic Anisotropy and Shear-Wave Splitting Using LPO Modelling

[9] The plastic deformation and textural evolution used in this study comes from the theory developed by *Ribe and Yu* [1991] and the theory of dynamic recrystallization from KR01.

[10] In the work by KR01 plastic deformation and dynamic recrystallization (via nucleation and grain boundary migration) experienced by an aggregate depends only on the deformation imposed externally by a large scale fluid flow field, which is describe by its velocity gradient tensor. Dynamic recrystallization is dependant upon the density of dislocations, which in turn is effected by the local stress field due to the applied fluid flow. In their approach the density of dislocations is a function of the dimensionless nucleation rate, $\lambda$*, and grain boundary mobility, M* (KR01). From comparisons with LPO obtained in experimental deformations of olivine aggregates the dimensionless nucleation rate has been estimated by KR01 to be $\lambda^* > 3$. They also constrain M* using the temporal evolution in the strength of the LPO so that M* = 125 ± 75. Dynamic recrystallization may induce large variations in the size of grains forming the aggregate. Therefore, *Kaminski et al.* [2004] incorporate grain boundary sliding via a dimensionless volume fraction $\chi$. If $\chi$ is close to zero then only a small fraction of grains deform by grain boundary sliding, whereas when $\chi$ is close to 1, all grains deform by grain boundary sliding and the distribution of orientations stays uniform. With torsional experiments at very large strains *Kaminski et al.* [2004] constrains the threshold dimensionless volume to be $\chi$ = 0.3 ± 0.1. LPO deformation is

therefore a balance between plastic deformation, dynamic recrystallization and grain boundary sliding.

[11] The model space is split into a series of nodes (the spacing is 40 km in both x and z directions) and LPO is calculated for an aggregate in response to an applied deformation at each node point. The aggregates are propagated backward through the velocity field until they exit the model at a depth of 410 km. At this depth, the LPO is assumed random or isotropic, having just passed through the phase transition at 410 km. The aggregates are then propagated through the velocity model to the original starting point, calculating the accumulated LPO at each time step and the aggregate volume fraction and orientation is outputted. We use Voigt averaging [*Mainprice*, 1990] and the projection method of *Browaeys and Chevrot* [2004] to calculate the best hexagonal approximation of the elastic tensors (widely used symmetry simplification in seismic studies) outputted from the LPO models. *Blackman et al.* [2002] show that when anisotropy is large (~10%) there can be differences in estimated seismic properties and traveltime anomalies between hexagonal symmetry and the lower symmetry classes. However we are trying to gauge sensitivity between different anisotropy models in this study and not to directly compare the results to observations, so we therefore use the hexagonal approximation.

[12] Seismic rays are traced using an anisotropic ray tracer [*Guest and Kendall*, 1993] that uses: P-wave velocity structure, S-wave velocity structure, density structure (from PREM [*Dziewonski and Anderson*, 1981]) and some description of anisotropy. In this study we use the Thomsen parameters [*Thomsen*, 1986] to describe the predicted seismic anisotropy. The Thomsen parameters are three measures of anisotropy, and provide an immediate estimate of anisotropy that is unavailable by simple inspection of the moduli themselves [*Thomsen*, 1986]. Each Thomsen parameter is set equal to the anisotropy calculated at each nodal point by the projection method of *Browaeys and Chevrot* [2004] and hence we assume elliptical anisotropy and by definition describe a transversely isotropic medium. The symmetry axis is aligned with the fast axis generated by the projection method of *Browaeys and Chevrot* [2004]. Sv and Sh rays are traced from 410 km depth along vertical ray paths (similar to SKS phases) to stations at the surface. Shear–wave splitting is simply the difference in travel time between Sh and Sv at each receiver.

## 4. Sensitivity of Shear-Wave Splitting to Mineral Parameters

[13] In the following modelling we use the flow field describe above and the mineral parameters are $\chi = 0.2$, $\lambda^* = 5$, $M^* = 125$, with an aggregate comprised of 70% olivine and 30% enstatite (composition of typical upper mantle material [*Anderson*, 1989]) which are suggested to be most Earth like by KR01 unless otherwise stated. Figure 1b shows the predicted anisotropy for the preferred mineral parameters.

[14] If temperature is the main controlling factor of grain boundary migration in the mantle then $M^* = 125 \pm 75$ (KR01). If $M^* = 50$ (Figure 1c), the generated seismic anisotropy exhibits similar patterns and orientations of the fast axis as for $M^* = 125$, but the strength of the predicted seismic anisotropy is reduced (max anisotropy only 9.08% compared to 9.43% in Figure 1b). When $M^* = 200$ (Figure 1d) the magnitude of seismic anisotropy has increased (max is 9.5%). For a larger grain boundary mobility, grains orientate faster towards the direction of material flow.

[15] Figures 2a and 2b shows the effect on predicted shear-wave splitting of varying the dimensionless grain boundary mobility. Although, the seismic anisotropy models show small differences in the magnitude of anisotropy, these changes do not appear to have a significant effect on the predicted shear-wave splitting. The maximum differences in shear-wave splitting between the models are ~0.05 secs. When $M^* = 200$ the predicted shear-wave splitting curve becomes erratic. This is due to the irregular nature of the predicted seismic anisotropy (small vortices can be seen in Figure 1d) at depth.

[16] Figures 1b, 1e, and 1f shows the effect on seismic anisotropy of varying the threshold volume for the activation of grain boundary sliding. An increase in seismic anisotropy (max seismic anisotropy increases from 9.4% to 11%) is observed when the threshold volume is decreased from $\chi = 0.2$ to $\chi = 0.0$ (Figure 1e). This magnitude of seismic anisotropy is larger than that expected for olivine (S-wave anisotropy measured for olivine rock samples generally saturates at 8–9% [*Ribe*, 1992]), and no grains are deforming by grain boundary sliding. When the threshold volume for the activation of grain boundary sliding is increased to $\chi = 0.4$ (Figure 1f), the maximum seismic anisotropy reduces from 9.4% to 7%. When the threshold volume is this high, the fraction of grains that deform by grain boundary sliding is large. Therefore, the seismic anisotropy produced is taking into account the contribution of small grains that deform via grain boundary migration.

[17] Figures 2c and 2d show the effect on predicted shear-wave splitting of varying the threshold volume for the activation of grain boundary sliding. The maximum difference between the predicted shear-wave splitting for $\chi = 0.2$ and $\chi = 0.4$ is only 0.05 secs. However, when $\chi$ are outside of this suggested range the predicted shear-wave splitting increases from 0.5secs near the ridge to in excess of 4secs off-axis. These magnitudes are produced because small grains are allowed to deform via dislocation creep instead of grain boundary sliding, thus the predicted seismic anisotropy and hence shear-wave splitting is larger than what is observed for aggregates of olivine and enstatite.

[18] Figures 1b and 1g shows that when only plastic deformation is considered, a lower seismic anisotropy (max 6–7%) is predicted compared to 9.4% for a model that also incorporates dynamic recrystallization. Generally, dynamic recrystallization is thought to randomise lattice-preferred orientations, thus reducing the magnitude of seismic anisotropy. However, *Blackman et al.* [2002] report that seismic anisotropy beneath mid-ocean ridges increases when dynamic recrystallization is incorporated in their models. The recrystallized grains re-orientate themselves to the direction of flow, and predict larger LPO and stronger seismic anisotropy. This effect is highlighted by the orientation of the fast axis (black bars). In the plastic deformation models the fast axis are not parallel to flow, whereas the recrystallized model predicts fast axis parallel to flow.

[19] Figure 2e shows the effect on predicted shear-wave splitting of varying the deformation processes being considered. The predicted shear-wave splitting results presented

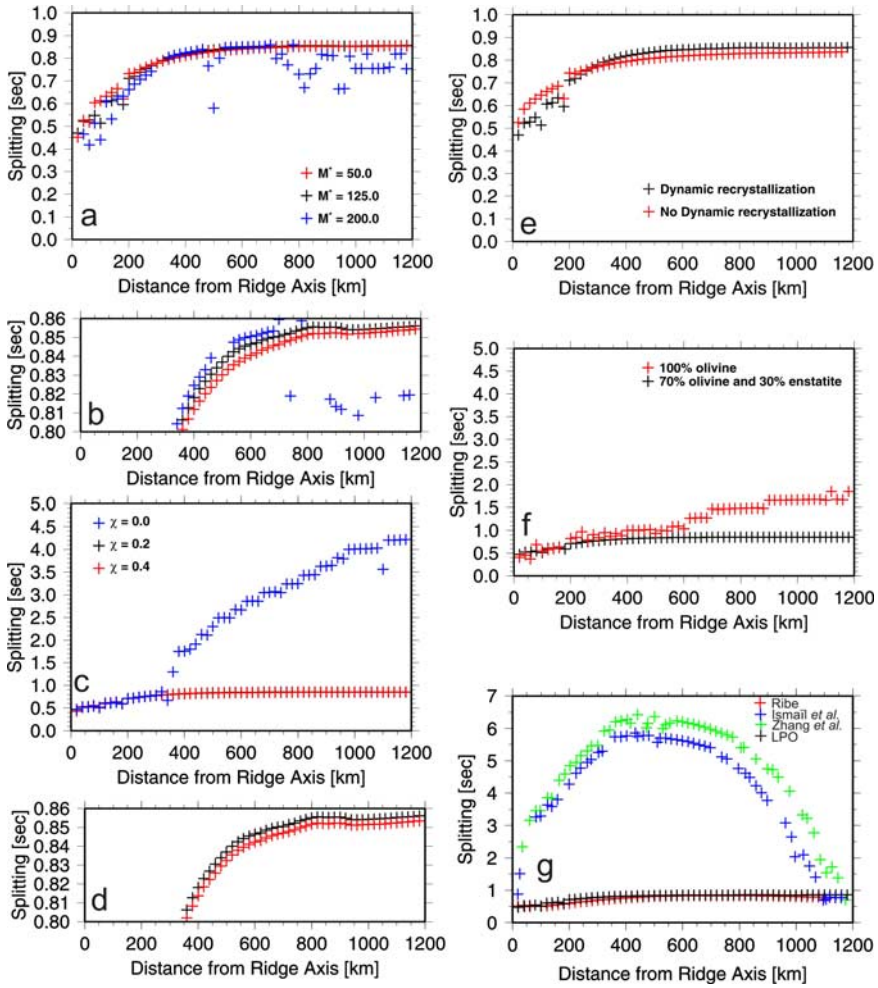


**Figure 2.** The predicted shear-wave splitting for a simple model of a mid-ocean ridge. (a–f) Sensitivity to mineral input parameters. Parameters are M* = 125, $\chi$ = 0.2, using dynamic recrystallization, and an aggregate composite comprising 70% olivine and 30% enstatite unless otherwise stated. (a–b) sensitivity to M*, (c–d) sensitivity to$\chi$, (e) sensitivity to dynamic recrystallization, and (f) sensitivity to aggregate mineralogy. (g) Sensitivity of predicted shear-wave splitting to the finite strain conversion scheme used at a mid-ocean ridge.

here show an interesting effect. Close to the ridge axis greater shear-wave splitting is produced by a model that deforms by plastic deformation only, while at distances off-axis the dynamic recrystallization model predicts greater shear-wave splitting. This confirms the results reported by *Blackman et al.* [2002] which state that in the off axis, where flow is similar to simple shear seismic anisotropy and hence shear-wave splitting increases when dynamic recrystallization is incorporated. Near the ridge axis however, the effect of dynamic recrystallization is to randomise LPO, and reduce the seismic anisotropy, thus reducing the predicted shear-wave splitting.

[20] Figures 1b and 1h show the effect on seismic anisotropy of varying the mineral composition of the aggregate. When the aggregate is comprised of purely olivine grains the maximum seismic anisotropy increases from 9.4% to > 11%. A well-known result of purely plastic deformation models [*Blackman et al.*, 2002] is that enstatite splitting maximum occurs ~20° from the *b-axis* as opposed to olivine where it occurs at 15–20° from the *c-axis*. Enstatite has only one active slip system, so that the density of dislocations is smaller than in olivine and there is less energy to drive dynamic recrystallization. Furthermore, the volume fraction of enstatite and thus its effective grain boundary mobility are smaller than those for olivine [*Kaminski et al.*, 2004]. The effect is that enstatite decreases the total seismic anisotropy without altering the pattern, which is what is observed in Figure 1h. This has been previously shown by *Tommasi* [1998]. They show simulations of LPO development in peridotitic aggregates as well as LPO data from naturally deformed peridotites that suggests the presence of enstatite does not modify olivine LPO patterns, but it does weaken the aggregate seismic anisotropy [*Tommasi*, 1998].

[21] Figure 2f shows the effect on predicted shear-wave splitting of varying the mineral composition. The model which is comprised of 100% olivine predicts shear-wave splitting that is in excess of 1 sec compared to only ~0.8 secs for a model comprised of 70% olivine and 30% enstatite. This confirms what *Tommasi* [1998] noted, that enstatite does not affect the orientation of the predicted LPO, but it does affect the magnitude. Therefore, it is

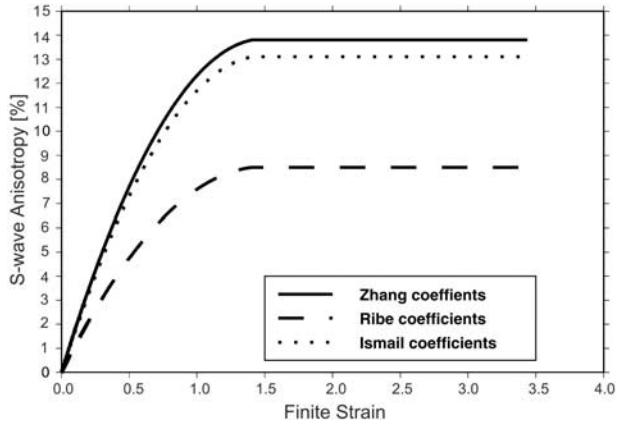


**Figure 3.** Finite strain to seismic anisotropy conversion schemes used in this study. Finite strain is calculated as the logarithm of the ratio of the long over short axis of the finite strain ellipse.

essential that enstatite be incorporated in upper mantle models of LPO, to achieve Earth-like observations.

[22] LPO predicted shear-wave splitting (with the preferred mineral parameters) is compared with that predicted using finite strain. We use the method described by *Nippress et al.* [2004] to calculate finite strain at each node point (the spacing is 40 km in both x and z directions) using the mantle flow above. The Thomsen parameters are assumed equal to the magnitude of the S-wave seismic anisotropy which is calculated using three different conversion schemes (Figure 3). The symmetry axis is aligned with the major axis of the finite strain ellipse. Figure 2g shows predicted shear-wave splitting for rays passing through seismic anisotropy models predicted using finite strain. When the conversion scheme of *Ribe* [1992] is used, predicted shear-wave splitting has the same magnitude ($\sim$0.8 secs) as that predicted by the LPO modelling. When the conversions to maximum anisotropies reported by *Zhang et al.* [2000] and *Ismaïl and Mainprice* [1998] are used however, the shear-wave splitting predictions are much greater and reach up to $\sim$6 secs in magnitude.

## 5. Discussion

[23] Observations of shear-wave splitting at mid-ocean ridges [e.g., *Wolfe and Silver*, 1998] are generally 0.45–1.5 secs in magnitude. Predicted shear-wave splitting using LPO (when M* and $\chi$ are within the bounds specified by KR01 and *Kaminski et al.* [2004], and with or without dynamic recrystallization) are consistent with observations. However the shear-wave splitting predicted by the simple isoviscous model used in this study would be expected to change if temperature and stress dependant viscosity, buoyancy and melt [*Braun et al.*, 2000, *Blackman et al.*, 2002] were incorporated in the flow modelling. In this study we allow anisotropy to develop in the upper 410 km, however seismic anisotropy may well only develop in the upper 200–300 km of the mantle where dislocation creep is dominant. We have modelled anisotropy accumulation in the upper 200 km of the mantle only and predict a similar seismic anisotropy pattern is predicted in the upper 200 km, however shear-wave splitting is reduced due to the shorter path length through this region. The control of shear-wave splitting by M*, $\chi$, dynamic recrystallization and mineral composition predicted in this study may be modified by the more complex mid-ocean ridge processes [*Braun et al.*, 2000, *Blackman et al.*, 2002] and the depth extent of dislocation creep. Factors controlling anisotropy may not be distinguishable observationally.

## 6. Summary

[24] We use a simplified mid-ocean ridge mantle flow model to investigate the sensitivity of predicted seismic anisotropy and shear-wave splitting to mineral parameters assumed in the LPO modelling technique. The mineral deformation and composition parameters used in the LPO modelling are shown to influence the predicted shear-wave splitting. The greatest influence is that of mineral composition of the mantle; when a pure olivine mantle is used, shear-wave splitting predictions are larger than seismic observations, implying that the effects of other minerals such as enstatite or garnet need to be considered. When experimentally derived ranges of mineral parameters (i.e. M*, $\lambda$*, $\chi$, and referenced resolved shear stresses) are used, while the predicted seismic anisotropy models exhibit variations, the predicted shear-wave splitting does not vary significantly and in a more complex tectonic environment such small variations may not be detectable. Seismic anisotropy and shear-wave splitting calculated from finite strain using the Ribe conversion are similar to those predicted by the LPO method using laboratory determined mineral parameters.

[25] **Acknowledgments.** Stuart Nippress was supported by NERC research grants NER/S/A/2001/06301 and NE/C000315/1. We would like to thank E. Kaminski for helpful discussion of the LPO theory and its implementation and for supplying the code used to convert LPO into seismic anisotropy. We would like to thank the anonymous reviewer for their useful comments that helped improved the quality of this paper.

## References

Anderson, D. L. (1989), *Theory of the Earth*, Blackwell Sci., Boston, Mass.
Batchelor, G. K. (1967), *An Introduction to Fluid Dynamics*, Cambridge Univ. Press, New York.
Blackman, D. K., J.-M. Kendall, P. R. Dawson, H.-R. Wenk, D. Boyce, and J. Phipps Morgan (1996), Teleseismic imaging of subaxial flow at mid-ocean ridges: Travel-time effects of anisotropic mineral texture in the mantle, *Geophys. J. Int.*, *127*, 415–426.
Blackman, D. K., H.-R. Wenk, and J. M. Kendall (2002), Seismic anisotropy of the upper mantle: 1. Factors that affect mineral texture and effective elastic properties, *Geochem. Geophys. Geosyst.*, *3*(9), 8601, doi:10.1029/2001GC000248.
Braun, M. G., G. Hirth, and E. M. Parmentier (2000), The effects of deep damp melt on mantle flow and melt generation beneath mid-ocean ridges, *Earth Planet. Sci. Lett.*, *176*, 339–356.
Browaeys, J. T., and S. Chevrot (2004), Decomposition of the elastic tensor and geophysical applications, *Geophys. J. Int.*, *159*, 667–678.
Chastel, Y. B., P. R. Dawson, H. R. Wenk, and K. Bennet (1993), Anisotropic convection with implications for the upper mantle, *J. Geophys. Res.*, *98*, 17,757–17,771.
Dziewonski, A. M., and D. L. Anderson (1981), Preliminary Reference Earth Model (PREM), *Phys. Earth Planet. Inter.*, *25*, 297–537.
Guest, W. S., and J.-M. Kendall (1993), Modelling waveforms in anisotropic inhomogeneous media using ray theory and Maslov asymptotic theory: Applications to exploration geophysics, *Can. J. Explor. Geophys.*, *29*, 78–92.
Ismaïl, W. B., and D. Mainprice (1998), An olivine fabric database: An overview of upper mantle fabrics and seismic anisotropy, *Tectonophysics*, *296*, 145–157.
Jessell, M. W. (1988), Simulation of fabric development in recrystallizing aggregates, 1. Description of the method, *J. Struct. Geol.*, *10*, 771–778.

Kaminski, E., and N. M. Ribe (2001), A kinematic model for recrystallization and texture development in olivine polycrystals, *Earth Planet. Sci. Lett.*, *189*, 253–267.

Kaminski, E., N. M. Ribe, and J. T. Browaeys (2004), D-Rex, a program for calculation of seismic anisotropy due to crystal lattice preferred orientation in the convective upper mantle, *Geophys. J. Int.*, *157*, 1–9.

Mainprice, D. (1990), A FORTRAN program to calculate seismic anisotropy from the lattice preferred orientation of minerals, *Comput. Geosci.*, *16*, 385–393.

Nicolas, A., and N. I. Christensen (1987), Formation of anisotropy in upper mantle peridotites: A review, in *Composition, Structure and Dynamics of the Lithosphere-Asthenosphere System*, *Geodyn. Ser.*, vol. 16, edited by K. Fuchs and C. Froidevaux, pp. 111–123, AGU, Washington, D. C.

Nippress, S. E. J., N. J. Kusznir, and J.-M. Kendall (2004), Modeling of lower mantle seismic anisotropy beneath subduction zones, *Geophys. Res. Lett.*, *31*, L19612, doi:10.1029/2004GL020701.

Phipps Morgan, J. (1987), Melt migration beneath mid-ocean spreading centers, *Geophys. Res. Lett.*, *14*, 1238–1241.

Ribe, N. M. (1992), On the relation between seismic anisotropy and finite strain, *J. Geophys. Res.*, *97*, 8737–8747.

Ribe, N. M., and Y. Yu (1991), A theory for plastic deformation and textural evolution of olivine polycrystals, *J. Geophys. Res.*, *96*, 8325–8335.

Thomsen, L. (1986), Weak elastic anisotropy, *Geophysics*, *51*, 1954–1966.

Tommasi, A. (1998), Forward modelling of the development of seismic anisotropy in the upper mantle, *Earth Planet. Sci. Lett.*, *160*, 1–13.

Wenk, H. R., and C. N. Tomé (1999), Modelling dynamic recrystallization of olivine aggregates deformed by simple shear, *J. Geophys. Res.*, *104*, 25,513–25,527.

Wenk, H. R., G. Canova, Y. Bruchet, and L. Flandin (1997), A deformation based model of recrystallization of anisotropic materials, *Acta Mater.*, *45*, 3283–3296.

Wolfe, C. J., and P. G. Silver (1998), Seismic anisotropy of oceanic upper mantle: Shear-wave splitting methodologies and observations, *J. Geophys. Res.*, *103*, 749–771.

Zhang, S., S. I. Karato, J. F. Gerald, U. H. Faul, and Y. Zhou (2000), Simple shear deformation of olivine aggregates, *Tectonophysics*, *316*, 133–152.

J.-M. Kendall, Earth Sciences, University of Bristol, Wills Memorial Bldg, Queens Road, Bristol BS8 1RJ, UK.

N. J. Kusznir and S. E. J. Nippress, Department of Earth and Ocean Sciences, University of Liverpool, 4 Bownlow Street, Liverpool L69 3GP, UK. (nippress@liverpool.ac.uk)